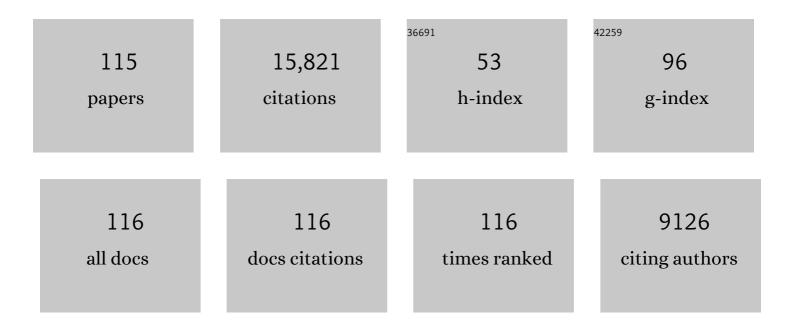
Howard A Zebker

List of Publications by Year in descending order

Source: https://exaly.com/author-pdf/2361653/publications.pdf Version: 2024-02-01



#	Article	IF	CITATIONS
1	Volcano geodesy using InSAR in 2020: the past and next decades. Bulletin of Volcanology, 2022, 84, 1.	1.1	17
2	A Signal Model for PRF Dithering in Wide-Swath, Fine-Resolution InSAR. IEEE Geoscience and Remote Sensing Letters, 2021, 18, 1214-1218.	1.4	2
3	A New Decorrelation Phase Covariance Model for Noise Reduction in Unwrapped Interferometric Phase Stacks. IEEE Transactions on Geoscience and Remote Sensing, 2021, 59, 10126-10135.	2.7	8
4	Accuracy of a Model-Free Algorithm for Temporal InSAR Tropospheric Correction. Remote Sensing, 2021, 13, 409.	1.8	18
5	Active layer thickness as a function of soil water content. Environmental Research Letters, 2021, 16, 055028.	2.2	35
6	Validation of Permafrost Active Layer Estimates from Airborne SAR Observations. Remote Sensing, 2021, 13, 2876.	1.8	9
7	Permafrost Dynamics Observatory—Part I: Postprocessing and Calibration Methods of UAVSAR Lâ€Band InSAR Data for Seasonal Subsidence Estimation. Earth and Space Science, 2021, 8, e2020EA001630.	1.1	11
8	Non-Gaussian Extensions for the Detection of Persistent Scatterers: Addressing the Limitations of Gaussian Models for InSAR Imagery. , 2021, , .		0
9	Permafrost Dynamics Observatory: Retrieval of Active Layer Thickness and Soil Moisture from Airborne Insar and Polsar Data. , 2021, , .		0
10	Backscatter Distributions of Persistent and Distributed Scatterers Over Wavelength: Results From <i>X</i> -, <i>C</i> -, and <i>L</i> -Band. IEEE Journal of Selected Topics in Applied Earth Observations and Remote Sensing, 2020, 13, 5518-5525.	2.3	6
11	A Physics-Based Decorrelation Phase Covariance Model for Effective Decorrelation Noise Reduction in Interferogram Stacks. , 2020, , .		2
12	The Case for 6-Hour Repeat Insar. , 2020, , .		1
13	Feasibility of Retrieving Soil Moisture from InSAR Decorrelation Phase and Closure Phase. , 2020, , .		5
14	On the Use of PRF Dithering for Wide Swath, Fine Resolution InSAR. , 2020, , .		0
15	An Analytical Framework for Understanding Persistent Scatterer Incidence in INSAR Imagery with Bandwidth and Wavelength. , 2020, , .		0
16	High-Pass Filters to Reduce the Effects of Broad Atmospheric Contributions in Sbas Inversions: A Case Study in the Delaware Basin. , 2020, , .		1
17	Joint Retrieval of Soil Moisture and Permafrost Active Layer Thickness Using L-Band Insar and P-Band Polsar. , 2020, , .		1
18	An Algorithm for Estimating and Correcting Decorrelation Phase From InSAR Data Using Closure Phase Triplets. IEEE Transactions on Geoscience and Remote Sensing, 2019, 57, 10390-10397.	2.7	25

#	Article	IF	CITATIONS
19	Inference of the impact of wildfire on permafrost and active layer thickness in a discontinuous permafrost region using the remotely sensed active layer thickness (ReSALT) algorithm. Environmental Research Letters, 2019, 14, 035007.	2.2	64
20	Persistent Scatterer Density by Image Resolution and Terrain Type. IEEE Journal of Selected Topics in Applied Earth Observations and Remote Sensing, 2019, 12, 2069-2079.	2.3	10
21	SAR Image Statistics by Bandwidth Using a Mixture Distribution of Persistent Scatterer and Clutter Distributions. , 2019, , .		2
22	Answers to Questions about User-Friendly Insar Data Products. , 2019, , .		1
23	Insar Mission-Level Products on Demand - do we Need Range-Doppler?. , 2018, , .		1
24	Persistent Scatterer Statistics and Their Detection. , 2018, , .		0
25	Estimating the permanent loss of groundwater storage in the southern <scp>S</scp> an <scp>J</scp> oaquin <scp>V</scp> alley, <scp>C</scp> alifornia. Water Resources Research, 2017, 53, 2133-2148.	1.7	96
26	Global drainage patterns and the origins of topographic relief on Earth, Mars, and Titan. Science, 2017, 356, 727-731.	6.0	39
27	Phase Correction of Single-Look Complex Radar Images for User-Friendly Efficient Interferogram Formation. IEEE Journal of Selected Topics in Applied Earth Observations and Remote Sensing, 2017, 10, 2694-2701.	2.3	19
28	User-Friendly InSAR Data Products: Fast and Simple Timeseries Processing. IEEE Geoscience and Remote Sensing Letters, 2017, 14, 2122-2126.	1.4	23
29	The Temporal and Spatial Variability of the Confined Aquifer Head and Storage Properties in the San Luis Valley, Colorado Inferred From Multiple InSAR Missions. Water Resources Research, 2017, 53, 9708-9720.	1.7	29
30	Robust and efficient insar deformation time series processing. , 2016, , .		1
31	4-Dimensional imaging from interferometric synthetic aperture radar. , 2016, , .		Ο
32	Ground-penetrating radar-derived measurements of active-layer thickness on the landscape scale with sparse calibration at Toolik and Happy Valley, Alaska. Geophysics, 2016, 81, H9-H19.	1.4	14
33	Confined aquifer head measurements and storage properties in the San Luis Valley, Colorado, from spaceborne InSAR observations. Water Resources Research, 2016, 52, 3623-3636.	1.7	57
34	Titan's "Magic Islands― Transient features in a hydrocarbon sea. Icarus, 2016, 271, 338-349.	1.1	37
35	Ground-penetrating radar-derived measurements of active-layer thickness on the landscape scale with sparse calibration at Toolik and Happy Valley, Alaska. Geophysics, 2016, 81, H1-H11.	1.4	3
36	A persistent scatterer interpolation for retrieving accurate ground deformation over InSARâ€decorrelated agricultural fields. Geophysical Research Letters, 2015, 42, 9294-9301.	1.5	19

#	Article	IF	CITATIONS
37	Remotely Sensed Active Layer Thickness (ReSALT) at Barrow, Alaska Using Interferometric Synthetic Aperture Radar. Remote Sensing, 2015, 7, 3735-3759.	1.8	59
38	Surface of Ligeia Mare, Titan, from Cassini altimeter and radiometer analysis. Geophysical Research Letters, 2014, 41, 308-313.	1.5	43
39	Groundwater extraction, land subsidence, and sea-level rise in the Mekong Delta, Vietnam. Environmental Research Letters, 2014, 9, 084010.	2.2	276
40	InSAR detects increase in surface subsidence caused by an Arctic tundra fire. Geophysical Research Letters, 2014, 41, 3906-3913.	1.5	64
41	An Analysis of the Uncertainty in InSAR Deformation Measurements for Groundwater Applications in Agricultural Areas. IEEE Journal of Selected Topics in Applied Earth Observations and Remote Sensing, 2014, 7, 2992-3001.	2.3	22
42	The 2010 slow slip event and secular motion at Kı̄lauea, Hawai‵i, inferred from TerraSARâ€X InSAR data. Journal of Geophysical Research: Solid Earth, 2014, 119, 6667-6683.	1.4	9
43	Estimating temporal changes in hydraulic head using InSAR data in the San Luis Valley, Colorado. Water Resources Research, 2014, 50, 4459-4473.	1.7	38
44	The bathymetry of a Titan sea. Geophysical Research Letters, 2014, 41, 1432-1437.	1.5	119
45	Shape, topography, gravity anomalies and tidal deformation of Titan. Icarus, 2014, 236, 169-177.	1.1	88
46	Reducing Ionospheric Effects in InSAR Data Using Accurate Coregistration. IEEE Transactions on Geoscience and Remote Sensing, 2014, 52, 60-70.	2.7	34
47	Phased arrays in time and space: A review. , 2013, , .		0
48	A global topographic map of Titan. Icarus, 2013, 225, 367-377.	1.1	70
49	Surface motion of active rock glaciers in the Sierra Nevada, California, USA: inventory and a case study using InSAR. Cryosphere, 2013, 7, 1109-1119.	1.5	61
50	Release of arsenic to deep groundwater in the Mekong Delta, Vietnam, linked to pumping-induced land subsidence. Proceedings of the National Academy of Sciences of the United States of America, 2013, 110, 13751-13756.	3.3	202
51	Characterization and identification of partially correlated persistent scatterers for InSAR remote sensing. , 2013, , .		0
52	InSAR Study of Shoreline Change along the Damietta Promontory, Egypt. Journal of Coastal Research, 2012, 284, 1263-1269.	0.1	10
53	Land subsidence in the Nile Delta of Egypt observed by persistent scatterer interferometry. Remote Sensing Letters, 2012, 3, 621-630.	0.6	31
54	Ionospheric Artifacts in Simultaneous L-Band InSAR and GPS Observations. IEEE Transactions on Geoscience and Remote Sensing, 2012, 50, 1227-1239.	2.7	20

#	Article	IF	CITATIONS
55	InSAR Deformation Time Series Using an \$L_{1}\$-Norm Small-Baseline Approach. IEEE Transactions on Geoscience and Remote Sensing, 2011, 49, 536-546.	2.7	101
56	High quality InSAR data linked to seasonal change in hydraulic head for an agricultural area in the San Luis Valley, Colorado. Water Resources Research, 2011, 47, .	1.7	40
57	Smoothing Criteria for Regularized Matrix Inversion of Bistatic Radar Echoes. Proceedings of the IEEE, 2011, 99, 895-905.	16.4	Ο
58	Comparison of Persistent Scatterers and Small Baseline Time-Series InSAR Results: A Case Study of the San Francisco Bay Area. IEEE Geoscience and Remote Sensing Letters, 2011, 8, 592-596.	1.4	59
59	InSAR detection of residual settlement of an ocean reclamation engineering project: a case study of Hong Kong International Airport. Journal of Oceanography, 2011, 67, 415-426.	0.7	34
60	Regional geomorphology and history of Titan's Xanadu province. Icarus, 2011, 211, 672-685.	1.1	52
61	Transient surface liquid in Titan's polar regions from Cassini. Icarus, 2011, 211, 655-671.	1.1	113
62	Cassini SAR, radiometry, scatterometry and altimetry observations of Titan's dune fields. Icarus, 2011, 213, 608-624.	1.1	74
63	Geodetically Accurate InSAR Data Processor. IEEE Transactions on Geoscience and Remote Sensing, 2010, 48, 4309-4321.	2.7	56
64	Detailed rockslide mapping in northern Norway with small baseline and persistent scatterer interferometric SAR time series methods. Remote Sensing of Environment, 2010, 114, 2097-2109.	4.6	133
65	Edgelist phase unwrapping algorithm for time series InSAR analysis. Journal of the Optical Society of America A: Optics and Image Science, and Vision, 2010, 27, 605.	0.8	61
66	Size and Shape of Saturn's Moon Titan. Science, 2009, 324, 921-923.	6.0	86
67	Cassini RADAR Sequence Planning and Instrument Performance. IEEE Transactions on Geoscience and Remote Sensing, 2009, 47, 1777-1795.	2.7	24
68	Sparse Two-Dimensional Phase Unwrapping Using Regular-Grid Methods. IEEE Geoscience and Remote Sensing Letters, 2009, 6, 327-331.	1.4	19
69	Sparse Two-Dimensional Phase Unwrapping Using Regular Grid Methods. IEEE Geoscience and Remote Sensing Letters, 2009, 6, 519-522.	1.4	12
70	Determining Titan surface topography from Cassini SAR data. Icarus, 2009, 202, 584-598.	1.1	108
71	Analysis and interpretation of Cassini Titan radar altimeter echoes. Icarus, 2009, 200, 240-255.	1.1	37
72	The shape of Saturn's moon Titan from Cassini radar altimeter and SAR monopulse observations. , 2009, , .		0

5

#	Article	IF	CITATIONS
73	Titan's surface from reconciled Cassini microwave reflectivity and emissivity observations. Icarus, 2008, 194, 704-710.	1.1	26
74	Titan's diverse landscapes as evidenced by Cassini RADAR's third and fourth looks at Titan. Icarus, 2008, 195, 415-433.	1.1	65
75	Titan's inventory of organic surface materials. Geophysical Research Letters, 2008, 35, .	1.5	184
76	Radar and Lidar Measurement of Terrestrial Processes. Eos, 2008, 89, 349-350.	0.1	10
77	Phase unwrapping in three dimensions with application to InSAR time series. Journal of the Optical Society of America A: Optics and Image Science, and Vision, 2007, 24, 2737.	0.8	305
78	ScanSAR-to-Stripmap Mode Interferometry Processing Using ENVISAT/ASAR Data. IEEE Transactions on Geoscience and Remote Sensing, 2007, 45, 3468-3480.	2.7	30
79	InSAR Remote Sensing Over Decorrelating Terrains: Persistent Scattering Methods. IEEE National Radar Conference - Proceedings, 2007, , .	0.0	11
80	Interferogram formation in the presence of complex and large deformation. Geophysical Research Letters, 2007, 34, .	1.5	58
81	Persistent scatterer selection using maximum likelihood estimation. Geophysical Research Letters, 2007, 34, .	1.5	59
82	Cryovolcanic features on Titan's surface as revealed by the Cassini Titan Radar Mapper. Icarus, 2007, 186, 395-412.	1.1	191
83	The lakes of Titan. Nature, 2007, 445, 61-64.	13.7	507
84	Estimating Snow Accumulation From InSAR Correlation Observations. IEEE Transactions on Geoscience and Remote Sensing, 2007, 45, 10-20.	2.7	46
85	Electrical properties of Titan's surface from Cassini RADAR scatterometer measurements. Icarus, 2007, 188, 367-385.	1.1	51
86	Measuring two-dimensional movements using a single InSAR pair. Geophysical Research Letters, 2006, 33, .	1.5	284
87	Titan Radar Mapper observations from Cassini's T3 fly-by. Nature, 2006, 441, 709-713.	13.7	95
88	Cassini RADAR observations of Enceladus, Tethys, Dione, Rhea, Iapetus, Hyperion, and Phoebe. Icarus, 2006, 183, 479-490.	1.1	76
89	Mapping of Titan: Results from the first Titan radar passes. Icarus, 2006, 185, 443-456.	1.1	49
90	Constraints on magma chamber geometry at Sierra Negra Volcano, Galápagos Islands, based on InSAR observations. Journal of Volcanology and Geothermal Research, 2006, 150, 232-243.	0.8	139

#	Article	IF	CITATIONS
91	The Sand Seas of Titan: Cassini RADAR Observations of Longitudinal Dunes. Science, 2006, 312, 724-727.	6.0	351
92	On trapdoor faulting at Sierra Negra volcano, Galápagos. Journal of Volcanology and Geothermal Research, 2005, 144, 59-71.	0.8	99
93	Cassini Radar Views the Surface of Titan. Science, 2005, 308, 970-974.	6.0	231
94	Accurate Estimation of Correlation in InSAR Observations. IEEE Geoscience and Remote Sensing Letters, 2005, 2, 124-127.	1.4	69
95	A new method for measuring deformation on volcanoes and other natural terrains using InSAR persistent scatterers. Geophysical Research Letters, 2004, 31, .	1.5	1,264
96	Inverse modeling of interbed storage parameters using land subsidence observations, Antelope Valley, California. Water Resources Research, 2003, 39, .	1.7	137
97	Prospecting for horizontal surface displacements in Antelope Valley, California, using satellite radar interferometry. Journal of Geophysical Research, 2003, 108, n/a-n/a.	3.3	29
98	Phase unwrapping for large SAR interferograms: statistical segmentation and generalized network models. IEEE Transactions on Geoscience and Remote Sensing, 2002, 40, 1709-1719.	2.7	527
99	Two-dimensional phase unwrapping with use of statistical models for cost functions in nonlinear optimization. Journal of the Optical Society of America A: Optics and Image Science, and Vision, 2001, 18, 338.	0.8	584
100	Seasonal subsidence and rebound in Las Vegas Valley, Nevada, observed by Synthetic Aperture Radar Interferometry. Water Resources Research, 2001, 37, 1551-1566.	1.7	297
101	Widespread uplift and â€~trapdoor' faulting on Galápagos volcanoes observed with radar interferometry. Nature, 2000, 407, 993-996.	13.7	300
102	Remote sensing of volcano surface and internal processes using radar interferometry. Geophysical Monograph Series, 2000, , 179-205.	0.1	54
103	Sensing the ups and downs of Las Vegas: InSAR reveals structural control of land subsidence and aquifer-system deformation. Geology, 1999, 27, 483.	2.0	501
104	High-Resolution Water Vapor Mapping from Interferometric Radar Measurements. Science, 1999, 283, 1297-1299.	6.0	155
105	A shallow-dipping dike fed the 1995 flank eruption at Fernandina Volcano, Galápagos, observed by satellite radar interferometry. Geophysical Research Letters, 1999, 26, 1077-1080.	1.5	76
106	Atmospheric effects in interferometric synthetic aperture radar surface deformation and topographic maps. Journal of Geophysical Research, 1997, 102, 7547-7563.	3.3	793
107	Analysis of active lava flows on Kilauea volcano, Hawaii, using SIR-C radar correlation measurements. Geology, 1996, 24, 495.	2.0	88
108	On the derivation of coseismic displacement fields using differential radar interferometry: The Landers earthquake. Journal of Geophysical Research, 1994, 99, 19617-19634.	3.3	512

#	Article	IF	CITATIONS
109	Mapping small elevation changes over large areas: Differential radar interferometry. Journal of Geophysical Research, 1989, 94, 9183-9191.	3.3	1,170
110	Satellite radar interferometry: Twoâ€dimensional phase unwrapping. Radio Science, 1988, 23, 713-720.	0.8	1,921
111	Imaging radar polarization signatures: Theory and observation. Radio Science, 1987, 22, 529-543.	0.8	476
112	Topographic mapping from interferometric synthetic aperture radar observations. Journal of Geophysical Research, 1986, 91, 4993-4999.	3.3	878
113	Saturn's rings: Particle size distributions for thin layer models. Icarus, 1985, 64, 531-548.	1.1	181
114	The microwave opacity of Saturn's rings at wavelengths of 3.6 and 13 cm from Voyager 1 radio occultation. Icarus, 1983, 54, 160-188.	1.1	86
115	Particle size distributions in Saturn's rings from voyager 1 radio occultation. Icarus, 1983, 54, 189-211.	1.1	145